



Synthesis, growth and physicochemical properties of new organic nonlinear optical crystal L-threoninium tartrate (LTT) for frequency conversion

S.E. Allen Moses^a, S. Tamilselvan^{a,*}, S.M. Ravi Kumar^b, G. Vinitha^c, Tejaswi Ashok Hegde^c, M. Vimalan^d, S. Varalakshmi^e, S. Sivaraj^b

^a PG & Research Department of Physics, Aringer Anna Government Arts College, Cheyyar 604 407, Tamil Nadu, India

^b PG & Research Department of Physics, Sri Subramaniaswamy Government Arts College, Tiruttani 631 209, Tamil Nadu, India

^c Division of Physics, School of Advanced Sciences, VIT, Chennai 600 127, Tamil Nadu, India

^d Department of Physics, Thirumalai Engineering College, Kanchipuram 631 551, Tamil Nadu, India

^e Department of Physics, Kamban College of Arts and Science for Women, Tiruvannamalai 606 601, Tamil Nadu, India

ARTICLE INFO

Article history:

Received 17 November 2018

Revised 6 May 2019

Accepted 6 May 2019

Available online 7 May 2019

Keywords:

Crystal growth

Optical properties

Dielectric

Laser damaged threshold

Third order nonlinear optical studies

ABSTRACT

An organic nonlinear optical L-threoninium tartrate (LTT) single crystal was successfully grown by slow evaporation method using de-ionized water as solvent. The orthorhombic structure and non-centrosymmetric space group of P222₁ of the grown LTT crystal was confirmed using single crystal X-ray diffraction analysis. The various functional groups and bonding nature of the LTT crystal were realized using FT-IR spectroscopic analysis. The linear optical behavior is examined using UV-Visible spectroscopy revealing the absences of absorbance in the wavelength region of 230–1100 nm. Tauc's relation is employed to obtain the optical band gap and it is found to be 6.4 eV. The optical parameters like extinction coefficient (K), reflectance (R) and refractive index (n₀) are also calculated for the grown LTT crystal. With respect to the frequency and temperature the dielectric constant and dielectric loss were estimated. The Vickers hardness number (H_v), Meyer's index (n), yield strength (σ_r), elastic constant (C₁₁), fracture toughness (K_C) and Brittle index number (B_i) were calculated using the micro-indentation test. Thermo-gravimetric (TG) and differential thermal (DT) analysis confirm the single stage decomposition and 257 °C melting point of the titular crystal. The exact melting point of the crystal is found to be 268 °C using auto melting point apparatus. The layer growth with 2D nucleation mechanism and less dislocation is confirmed by chemical etching analysis. The surface quality of the titular crystal was studied using laser damage threshold (LDT) measurement and it is found to be 6.57 GW/cm². Kurtz and Perry method was employed to estimate the second harmonic generation efficiency of the titular crystal and is found to be 2.91 times greater than the KDP crystal. The χ⁽³⁾, n₂ and β of the titular crystal was estimated using Z-scan technique and they are found to be 7.1368 × 10⁻¹⁰ (esu), 0.8466 × 10⁻¹² (cm²W⁻¹) and 3.734 × 10⁻⁶ (cmW⁻¹) respectively. Reverse saturable absorption observed in open aperture Z-scan indicates the suitability of titular crystal for optical limiting application.

© 2019 The Authors. Production and hosting by Elsevier B.V. on behalf of KeAi Communications Co., Ltd. This is an open access article under the CC BY-NC-ND license (<http://creativecommons.org/licenses/by-nc-nd/4.0/>).

* Corresponding author at: PG & Research Department of Physics, Aringer Anna Government Arts College, Cheyyar 604 407. Thiruvannamalai Dist., India.

E-mail address: stsresearch1977@gmail.com (S. Tamilselvan).

Peer review under responsibility of KeAi Communications Co., Ltd.



Production and hosting by Elsevier

1. Introduction

Second order nonlinear optical materials continue to be an important area of research due to its potential applications in various fields of optoelectronics, photonics and telecommunication [1]. So far inorganic materials with second-order nonlinear optical (NLO) susceptibilities were used as nonlinear optical materials such as lithium triborate (LBO), potassium dihydrogen phosphate (KDP), potassium niobate (KNbO₃), lithium niobate (LiNbO₃) [2–6]. Recently organic materials have drawn the attention of

researchers due to their large second-order nonlinear optical susceptibility and high laser damage threshold. Hence organic crystals are accepted to be an efficient NLO material [7,8]. Organic materials provide a strong charge transfer and high polarizability leading them to high nonlinearity and also organic crystals provide a good second harmonic conversion in ultraviolet and visible region which leads them for many device fabrications in optoelectronics and photonics [9–11]. The enormous optical and spectacular properties of the organic crystals motivated us to find new organic NLO crystals. Generally, organic based salts of amino acids exhibit very good nonlinear optical property because of the presence of proton donor carboxyl acids (^-COO) group and the proton acceptor (NH_2) group [12,13]. For the past few decades, many researchers reported on amino acid based materials like L-threoninium sodium fluoride, L-prolinium tartrate, L-arginine acetate, L-threonine acetate, etc. [2,14–16], due to their excellent NLO properties. Hence extensive research has been carried out for finding an alternative for inorganic materials into organic materials due to their higher nonlinear responsiveness and greater optical damage thresholds [17].

In this manuscript, a systematic study was carried out on the synthesis and growth of an organic L-threoninium tartrate (LTT) crystal by slow evaporation method using double distilled water as the solvent. The crystal structure determination, functional group identification (FT-IR), optical transmittance (UV), thermal stability (TGA/DTA), laser damaged threshold (LDT), mechanical behavior, etching, second harmonic generation (SHG) and third order nonlinear optical studies have been carried for the titular crystal for the first time and the results were discussed in detail.

2. Experimental

2.1. Synthesis

L-threoninium tartrate (LTT) has been synthesized using L-threonine and L-(+)-tartaric acid purchased from Lobo chemical 98.9% of purely. An equimolar ratio of the substance of L-threonine ($C_4H_9NO_3$) and L-(+)-tartaric acid ($C_4H_6O_6$) was dissolved in aqueous solution (deionized water) at room temperature. The solution was stirred for 8 h to attain homogenous mixture of L-threoninium tartrate solution. The reaction scheme of L-threoninium tartrate is shown in Fig. 1. The prepared solution was clarified using a filter paper and beaker covered with a mica sheet with few pin holes on it for slow evaporation in room temperature which leads to super-saturation.

The LTT crystal was obtained in a growth period of 80 days. A good quality hexagonal shape transparent crystal of LTT with dimension $11 \times 3 \times 3 \text{ mm}^3$ was obtained. Photograph of the LTT crystal is shown in Fig. 2.

3. Result and discussion

3.1. Single crystal X-ray diffraction studies

The unit cell parameters of the grown LTT crystal are estimated using Bruker single crystal Kappa APEXII-X-ray

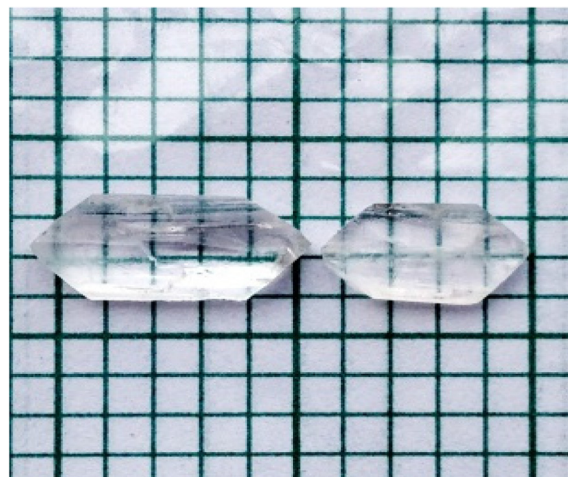


Fig. 2. Photograph of the grown LTT crystal.

diffractometer. From the analysis, it is observed that the LTT crystal crystallizes in the orthorhombic crystal system with a space group of $P222_1$. The estimated cell parameters of LTT are, $a = 5.157 \text{ \AA}$, $b = 7.757 \text{ \AA}$, $c = 13.636 \text{ \AA}$, $\alpha = \beta = \gamma = 90^\circ$ and the cell volume is 545.478 \AA^3 .

3.2. FT-IR studies

The grown crystal of LTT was subjected to FT-IR spectroscopy in order to analysis the functional groups present in it. The sample was powdered and recorded using KBr pellet technique, in the frequency range of $4000\text{--}400 \text{ cm}^{-1}$ using Jasco 410 spectrometer at a scanning rate of 2 mm/s at a resolution of 4 cm^{-1} . The recorded FT-IR spectrum is depicted in Fig. 3. The recorded FT-IR spectrum is compared with standard functional groups of pure compounds (L-threonine and L-tartaric acid) and grown sample LTT are tabulated in Table 1. The wave number 3404 cm^{-1} and 3154 cm^{-1} of L-tartaric acid and L-threonine were disappeared and shifted in between to a new wave number 3169 cm^{-1} due to NH_3^+ asymmetric stretching. The wave number 3021 cm^{-1} is due to O–H stretching. The absorption band at 2976 cm^{-1} and 2875 cm^{-1} are due to NH_3^+ and CH_2 stretching pure L-threonine [18]. A broadband at 2050 cm^{-1} is due to CN stretching. The very strong peak at 1736 cm^{-1} indicates the presence of C=O group, which confirms the presence of L-tartaric acid [19,20]. The broad peak at 1627 cm^{-1} is assigned to NH_3^+ asymmetric bending. The peaks at 1456 cm^{-1} and 1347 cm^{-1} are mixed deformation vibration of OH- and CH-present in alcohol group of tartaric acid [19,20]. The band at 932 cm^{-1} is due to CH_2 rocking vibration. The strong peak observed at 769 cm^{-1} is due to CO_2^- bending vibration. The sharp peak observed at 560 cm^{-1} due to CO_2^- rocking [21]. FT-IR spectrum of LTT reveals the presence of various functional groups of both L-threonine and L-tartaric acid in L-threoninium tartrate (LTT).

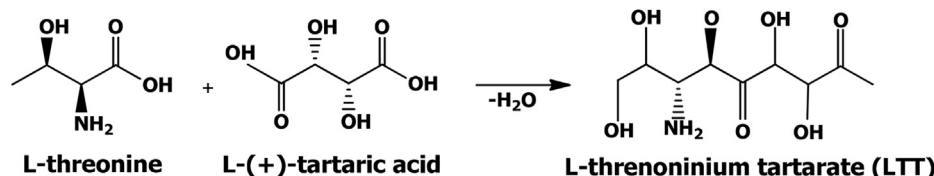


Fig. 1. Reaction scheme of LTT crystal.

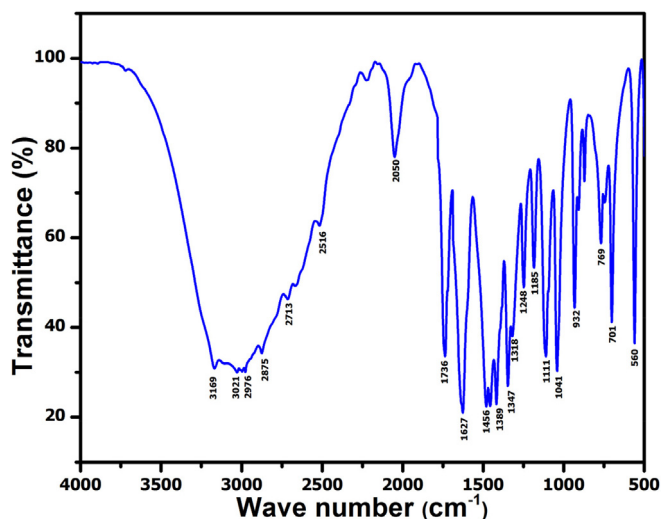


Fig. 3. FT-IR spectrum of LTT crystal.

Table 1
Comparative FT-IR vibrational assignments.

L-threonine [18]	L-tartaric acid [19,20]	L-threoninium tartrate (LTT) [Present work]	Assignments
–	3404	–	O–H stretching
3157	–	3169	NH ₃ ⁺ asymmetric stretching
–	–	2050	CN stretching
–	1737	1736	C=O stretching
1623	–	1627	NH ₃ ⁺ asymmetric bending
–	1450	1456	C–O stretching and O–H deforming
–	1399	1347	C–H stretching
931	903	932	CH ₂ rocking
767	789	769	CO ₂ bending
–	575	560	CO ₂ rocking

3.3. UV–Visible–Near IR studies

An optical transmittance studies is a key factor to determine the optical parameters of the titular crystal. The nonlinear optical crystal should have low absorption of light in the visible region and good transparency over near IR region in order to promote low

energy electrons to high energy state and these parameters are suitable for NLO oriented device fabrications. The optical properties of LTT crystal are studied by UV–Vis–NIR spectrum analysis using Perkin-Elmer Lambda-35 spectrometer in the wavelength range of 200–1100 nm, which covers UV (200–400 nm), visible (400–800 nm) and near IR (800–1100 nm) regions. The recorded transmission and absorption spectrums are shown in Fig. 4. The compound is active in the whole visible region with 97% transmittance. The transmittance spectra of the titular compound confirm no absorbance in the wavelength range between 250 and 1100 nm, which is due to the electronic transitions between the carboxylate (COO[–]) and nitril (NH₃⁺) bonds [18,22]. The lower cut-off wavelength of LTT crystal is found to be 190 nm from the absorbance graph. The spectra provide details about the structure of the molecule due to the direct involvement of electromagnetic wave the absorption in near UV region from $\pi \rightarrow \pi^*$ electron transition within the sample by carbonyl group [23,24]. LTT crystal provides good transparency, which is a suitable condition for SHG employed in Nd: YAG laser applications, Gallium arsenide (GaAs) for photonic and optical devices applications [18]. The value of the absorption coefficient (α) is measured using transmittance (T) data by using Eq. (1)

$$\alpha = \frac{2.303}{t} \log \frac{1}{T} \quad (1)$$

where 'T' is transmittance (%) and 't' is thickness is the crystal subjected UV analysis. The optical band gap (E_g) energy of LTT crystal is calculated using the Tauc's plot Eq. (2) [25].

$$(\alpha h\nu) = A(E_g - h\nu)^{\frac{1}{2}}, \quad (2)$$

where 'h' is Planck's constant, 'v' is frequency and 'A' is a constant. The Tauc's plot between $(\alpha h\nu)^2$ and $(h\nu)$ is shown in Fig. 5. From the plot, the optical band gap is found to be 6.4 eV. Wider band gap reveals the titular crystal belongs to the better optical material category with greater transmittance throughout the visible region, which is suitable for optoelectronic device fabrication [2]. To calculate the extinction coefficient (K), Eq. (3) is used and it was found to be 232.2 at 532 nm.

$$K = \frac{\alpha \lambda}{4\pi} \quad (3)$$

To calculate the reflectance (R) in terms of absorption coefficient the following expression (4) is used and it has been found to be R = 1.493 at 532 nm.

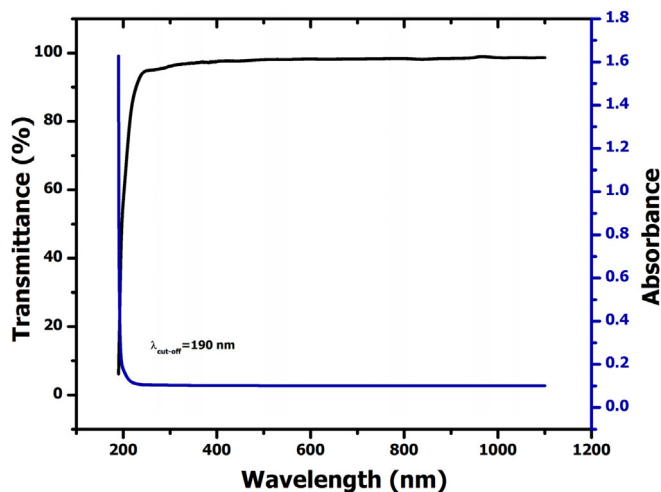
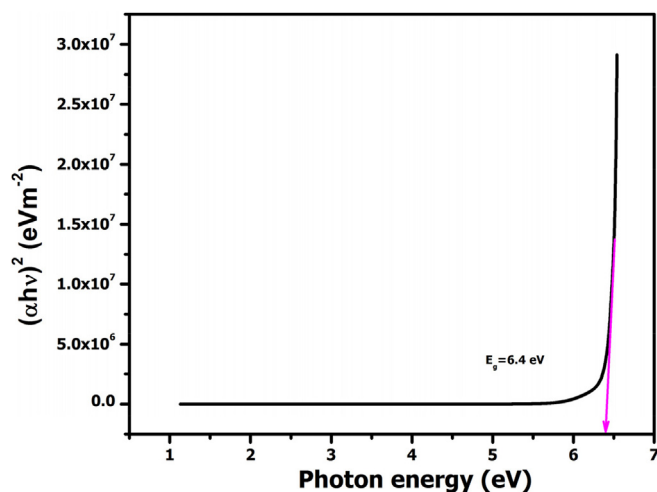


Fig. 4. Optical transmittance and absorption spectrums of LTT crystal.

Fig. 5. Photon energy versus $(\alpha h\nu)^2$ of LTT crystal.

$$R = e^{(-\alpha t)} \pm \sqrt{\frac{e^{(-\alpha t)}T - e^{(-3\alpha t)}T + e^{(-2\alpha t)}T^2}{e^{(-\alpha t)} + e^{(-2\alpha t)}T}} \quad (4)$$

By using the reflectance data, the refractive index (n_0) can be calculated using the expression (5).

$$n_0 = -(R + 1) \pm \frac{2\sqrt{R}}{(R - 1)} \quad (5)$$

The variation of reflectance (R) and refractive index (n_0) as a function of wavelength is shown in Fig. 6. The graph reveals that there is a decrease in refractive index (n_0) and extinction coefficient (K) with increasing in wavelength and the value of refractive index specify there is an absorbance in lower wavelength region due to the interaction between electrons and photos. The calculated refractive index (n_0) is found to be 1.83 at 532 nm and the refractive index and extinction coefficient are effectively wavelength dependent.

3.4. Dielectric studies

Dielectric measurement is important to understand the electrical properties of solids which give details about the nature of atoms, ions, phase change, and polarization. The material is polarized easily by an external electric field which is useful to measure the dielectric permittivity (ϵ) [26]. A good crystal with suitable size was chosen and polished on both sides using a silk cloth. The polished crystal with a thickness of 3 mm was placed in between the electrodes with silver paste in order to ensure good electrical contact. This dielectric medium of electrodes with crystal acts as a parallel plate capacitor. The capacitance of the grown crystal was studied in the frequency range in between 50 Hz and 5 MHz at various temperatures (313–343 K). The dielectric constant of LTT crystal was calculated using Eq. (6)

$$\epsilon = \frac{C_p t}{\epsilon_0 A} \quad (6)$$

where ‘ ϵ ’ is dielectric permittivity, ‘C’ is capacitance, ‘t’ is the thickness of the crystal, ‘ ϵ_0 ’ is the permittivity of free space and ‘A’ is area of the cross section of the crystal. The electric field distribution and charge transport mechanism can be understood clearly from the frequency dependence of the dielectric response of the crystal. The frequency dependent dielectric constant exhibits the four types of polarization in the sample namely ionic, electronic, orientation and space charge polarization. The increase of frequency with the

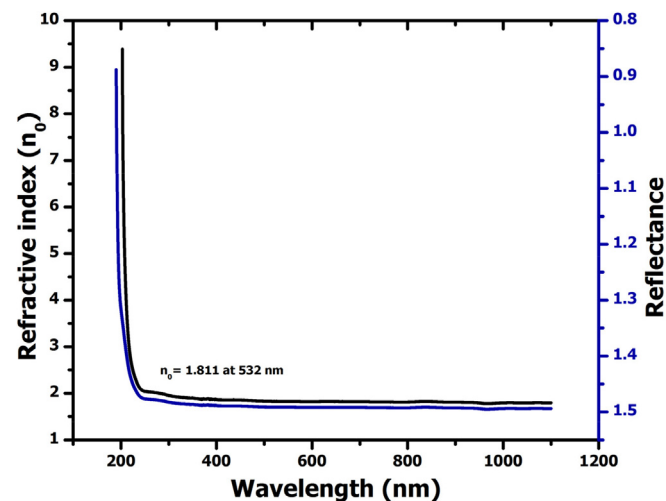


Fig. 6. Wavelength versus reflectance (R) and refractive index (n_0) of LTT crystal.

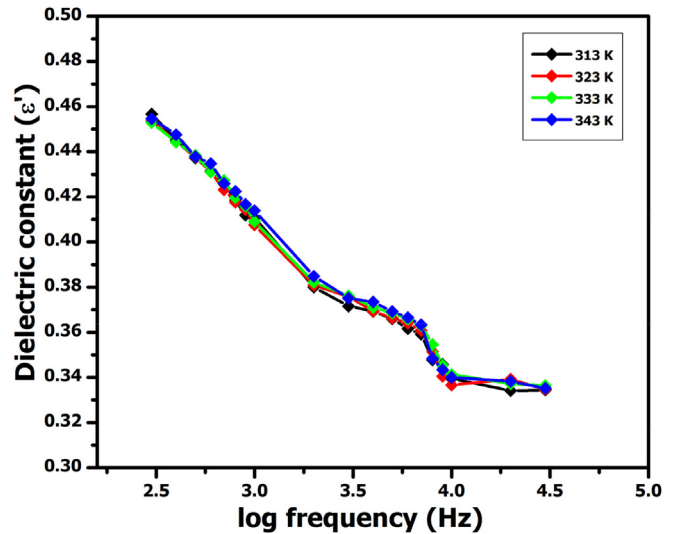


Fig. 7. Log frequency versus dielectric constant.

decrease of dielectric constant is depicted in Fig. 7. At low frequency, the dielectric constant shows greater values due to the presence of the space charge polarization. The space charge polarization mainly depends on three factors namely purity, perfection and high-temperature resistivity. At higher frequency, lower dielectric values indicate low power dissipation which is highly essential for electro-optic applications. The plot between dielectric loss versus log frequency is given in Fig. 8. The plot clearly specifies that the dielectric loss decays with enhancing in frequency for all temperature range. At high frequencies, low dielectric loss indicates the crystal possesses a wide optical quality and lesser number of defects [27]. From these parameters, it has been proved that the grown LTT crystal is a suitable candidate for NLO and electro-optic devices applications [28].

3.5. Mechanical properties

It is important to understand the mechanical behavior of the grown LTT crystal for optical and electronic device fabrication. Vickers microhardness (H_v), Meyer index (n), elastic constant (C_{11}), fracture toughness (K_C), Brittleness index number (B_i), Knoop hardness (H_k), corrected hardness (H_o) and yield strength (σ_T) are

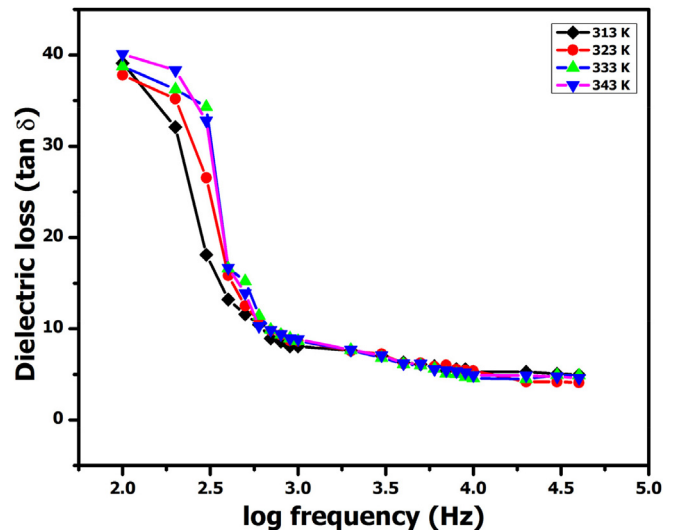


Fig. 8. Log frequency versus dielectric loss of LTT crystal.

some of the important parameters helps to understand the mechanical property some more better [29,30].

LTT crystal of thickness 3 mm had been chosen for the hardness test. The test had been carried out for varying loads from 25, 50, 100 g. The diagonal length (d) depends on impressions obtained

by varying loads which can be measured using micrometer for every load, three best impressions are taken and the average was considered. To find out the Vickers microhardness studies (H_v) the expression (7) was used. The graph drawn in between H_v versus $\log P$ is shown in Fig. 9(a).

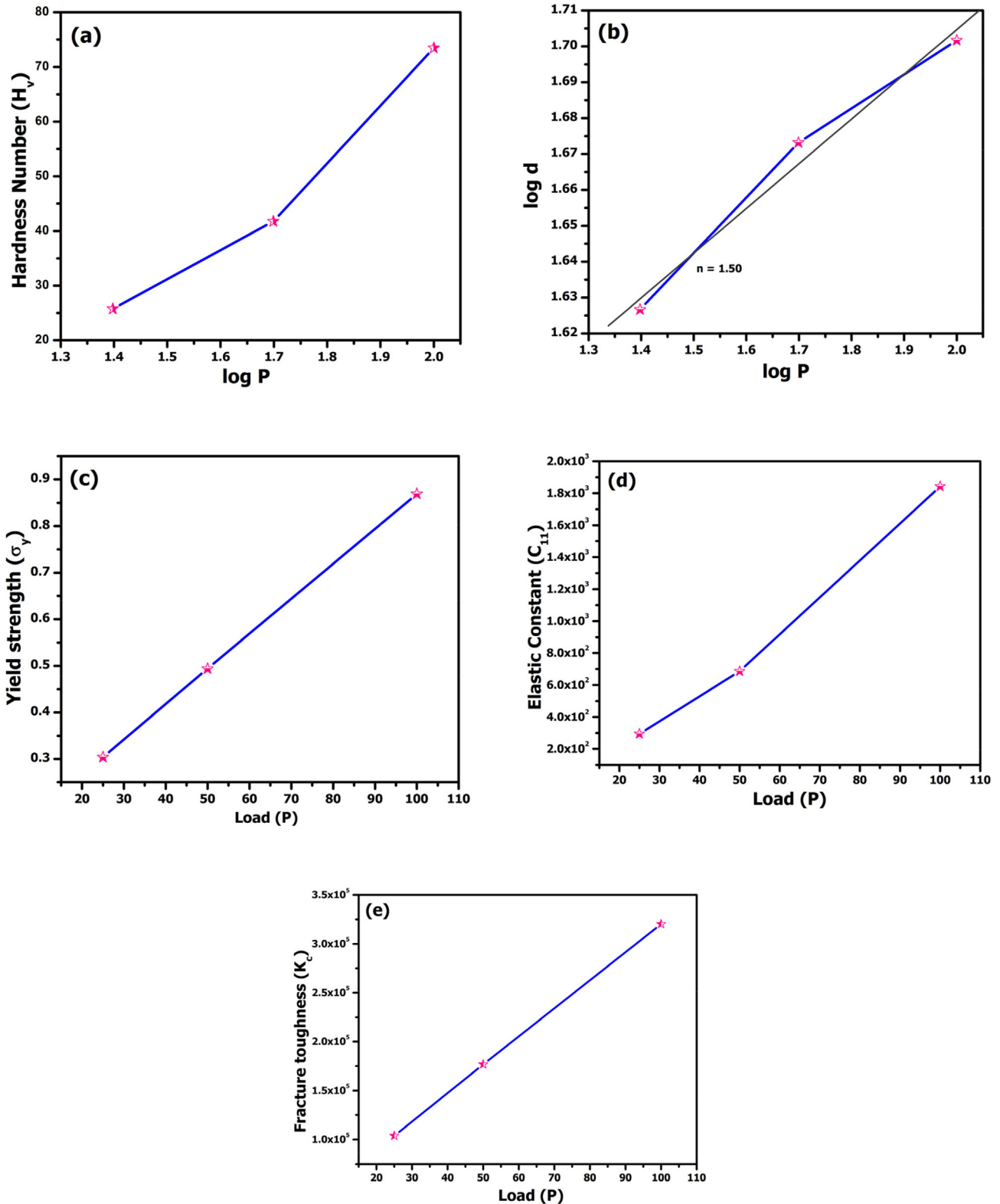


Fig. 9. (a) Log (P) versus hardness number (H_v), (b) Log (P) versus Log d , (c) applied load (P) versus yield strength (σ_y), (d) applied load (P) versus elastic constant (C_{11}), (e) applied load (P) versus fracture toughness (K_c) of the LTT crystal.

$$H_v = 1.8544 \times \frac{P}{d^2} \text{ (kg/mm}^2\text{)} \quad (7)$$

It is clear from the plot that H_v increases with increasing load P . This impact is known as reverse indentation size effect (RISE). For RISE on a specimen will not give resistance or elasticity, but it undergo relaxation with the release of the indentation stress leads to a huge indentation size with low hardness at minimum load [31]. The load is slowly increased from 25 g, 50 g, and 100 g, when the load reaches 100 g, mild cracks were observed around the indentation mark due to the internal stress by reducing the hardness [32]. The nature of the crystal either hard or soft category was determined using the following Meyer's law,

$$P = k_1 d^n \quad (8)$$

where ' k_1 ' is material constant, ' n ' is Meyer's index. This gives the relationship between load and indentation diagonal length. The graph is drawn between $\log p$ versus $\log d$ shown in Fig. 9(b). Slope value (n) is calculated as Meyer's number [33] and it is found to be 1.50. For harder materials, the value of ' n ' lies in between 1 and 1.6. Above 1.6 the material is considered as softer material [34,35]. So the study reveals the LTT crystal belongs to a harder category.

Keeping the n value it is easy to calculate the yield strength (σ_y) of the material. The value of yield strength depends on Mayer's index number. For $n > 2$ yield strength can be calculated using Eq. (9)

$$\sigma_y = \frac{3-n}{2.9} \times \left(\frac{[12.5(n-2)]}{3-n} \right)^{n-2} H_v \quad (9)$$

If, $n < 2$ expression (10) is used to calculate the yield strength.

$$\sigma_y = \frac{H_v}{3} \quad (10)$$

From the plot, it is clear that yield strength increases with increasing load as shown in Fig. 9(c). The binding of bonding between neighboring atoms is calculated using Wooster's empirical equation [36]. To find out the stiffness constant or elastic stiffness constant (C_{11}) the Eq. (11) can be used.

$$C_{11} = H_v^{7/4} \quad (11)$$

The variation of elastic stiffness constant (C_{11}) with load (P) is shown in Fig. 9(d). The stiffness constant gives the property of the strength and bonding nature with neighboring atoms. The resistance of fracture is indicated by fracture toughness (K_c). Eq. (12) was used to determine the toughness of material under uniform stress and load [37]. The plot between fracture toughness (K_c) and the applied load is depicted in Fig. 9(e).

$$K_c = \frac{P}{\beta_0 l^{3/2}} \text{ for } l \geq \frac{d}{2} \quad (12)$$

where β -constant depend upon indentation geometry for Vickers indenter ($\beta = 7$). Brittle index explains about the fracture-induced in the sample without external force. The Brittle index B_i can be calculated using Eq.(13).

$$B_i = \frac{H_v}{K_c} \quad (13)$$

The calculated values of Brittleness index (B_i), Vickers micro-hardness (H_v), yield strength (σ_y), elastic stiffness constant (C_{11}) and fracture toughness (K_c), are presented in Table 2.

3.6. Thermal analysis

It is important to know the thermal stability of the nonlinear optical crystals because thermal stability plays a vital role in device fabrication. Many electronic devices generate heat while functioning. Excellent thermal withstands of the crystal provides an accurate output [38]. The thermogram analysis of LTT crystal is carried out using TG/DTA analysis. A powder sample of 3.097 mg is taken for analysis between the temperature ranges of about 60 °C–800 °C in a nitrogen atmosphere. The recorded thermogram is depicted in Fig. 10. TGA spectrum shows a first decomposition observed at 228 °C with a weight loss of 5.1% due to the evaporation of water molecule from the crystal [14]. Second decomposition starts from 229 °C and ends around 302 °C with weight loss of 91.3%, remaining (4.6%) attributed to volatile residue formed by organic salts of LTT [39]. The endothermic peak at 257 °C of DTA represented the titular crystal melting point. Below 257 °C no endothermic/exothermic peaks were observed, which reveals the titular crystal provides a single decomposition point with greater thermal stability up to 257 °C which is a most acceptable temperature for high energy laser applications.

Also, Esico International auto melting point apparatus – 1935 is used to find an accurate melting point temperature of LTT crystal. The device is fabricated using advanced engineering microcontroller technology with enhanced accuracy. The melting of the LTT crystal is found to be 268 °C which is comparable with DTA value.

3.7. Etching analysis

Etching analysis is one of the easy and effective methods to identifying the growth defect of the grown crystal. Nonlinear effi-

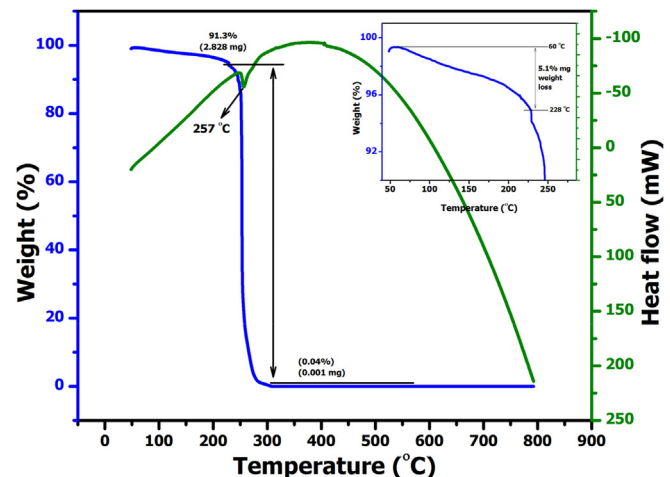


Fig. 10. TGA/DTA curves of LTT crystal.

Table 2
Calculated mechanical parameters of LTT crystal.

Load P (g)	H_v (kg/mm ²)	σ_y (GN/m ²)	$C_{11} \times 10^{14}$ (Pa)	$K_c \times 10^4$ (kg/m ^{3/2})	B_i (μ /m ^{1/2})
25	25.750	8.583	294.347	10.374	248.217
50	41.750	13.916	685.723	17.668	236.303
100	73.450	24.483	1842.832	32.025	229.352

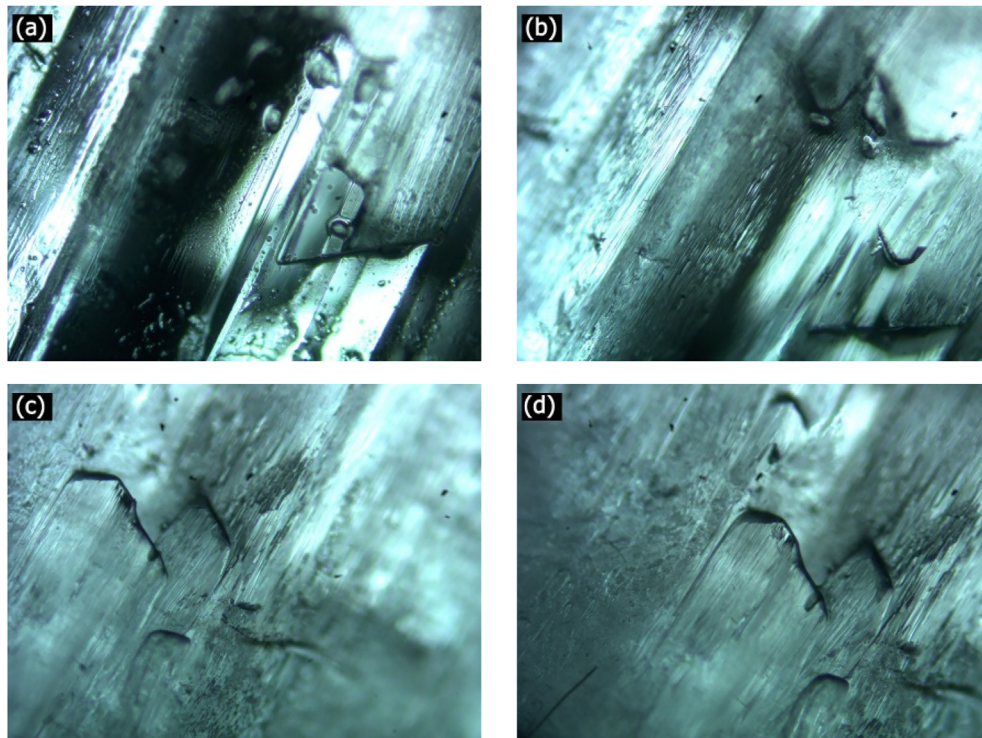


Fig. 11. Etch patterns for (a) as grown, (b) 10 s, (c) 20 s and (d) 30 s of LTT crystal.

ciency depends on the quality of crystal or well-defined defect structures for technical application and device fabrication. Transparent with crack free well sized as-grown crystal was chosen for this study. The etching study was carried out using deionized water as an etchant. The crystal was dipped in the etchant for 10 s, 20 s, and 30 s. The etched surface was immediately wiped using an unpigmented tissue paper. Then the crystal was analyzed by Carl Zeiss optical microscope in reflection mode at a lower magnification of $400\times$. Fig. 11(a)–(d) shows some well-defined trapezium etching pits with elongated lines. Increasing the duration from 20 to 30 s the observed trapezium pits were dislocated new layer etching pattern was formed which conforms the grown crystal has layer growth with 2D nucleation mechanism [40] with less dislocation which represents a good crystalline perfection.

3.8. Laser damage threshold measurement.

Laser damage threshold measurement is a determining factor for nonlinear device fabrication such as THz wave generation and electro-optic modulation and optical applications [41,42]. The nonlinear optical property depends on the surface quality of the crystal. Crystal with low surface damage by high power laser will affect its nonlinear property and its applications. So LDT measurement is carried out to test the optical breakdown, surface quality, performance and its withstanding power intensity with high power laser. Laser damage threshold effectiveness is depending upon various parameters such as surface quality, laser pulse width, laser energy, wavelength, etc. [43]. The laser damaged threshold measurement was carried out on LTT single crystal using Q – switched high energy Nd: YAG laser of wavelength 1064 nm with a pulse width of 6 ns and repetition rate of 10 Hz is used. The diameter of the laser beam is 0.8 mm. The output is controlled by variable attenuator and given to the crystal which is mounted on a sample holder at a focus of a biconvex lens with a focal length 150 mm. The input laser beam is given as pulse energy range 1.5 mJ–3 J and the laser damaged value for LTT single crystal is found to 6.57 GW/cm^2

Table 3

Comparison of LDT with some pre-reported NLO crystals.

Crystal	LDT (GW/cm ²)	References
KDP	0.20	[44]
L-threonine	2.22	[45]
L-threoninum sodium fluoride	4.10	[2]
L-threoninum phosphate	4.92	[46]
L-tartaric acid	5.4	[20]
L-prolinium tartrate	5.9	[14]
L-threoninum tartrate	6.57	[Present work]

which is quite higher than the pre-reported amino acids crystals. The LDT value of LTT crystal is compared with some previously reported NLO crystal in Table 3.

3.9. Nonlinear optical properties

Second harmonic generation (SHG) test was carried out to evaluate NLO property of the LTT crystal using Kurtz and Perry power technique [47]. The sample was illuminated by an intense beam of a wavelength of 1064 nm from Q-switched high energy Nd: YAG laser with an input energy pulse rate of 0.70 J, pulse width of 6 ns at a repetition rate of 10 Hz was used as a source. Initial calibration was done using the reference sample of KDP. A filtered IR beam was used as a fundamental input beam (0.70 J) with a photomultiplier tube (PMT) as a detector allowing the beam to pass through the powdered sample loaded in a microcapillary tube. The illumination beam was allowed to incident on the sample, output light was collected by the PMT conforming SHG signal of output 8.91 mJ. The SHG signal always depends on the crystals molecular structure and charge transfer between bonding groups [48,49]. The same procedure is repeated for the titular crystal and it was found to be 25.90 mJ, which is 2.91 times than that of the KDP crystal. A

Table 4
SHG result comparison with pre-reported amino acid crystals.

Compound	SHG efficiency	References
L-threoninium tartrate	2.91	[Present work]
L-threoninium phosphate	2.1	[46]
L-threonine	1.15	[18]
L-threonium acetate	1.14	[16]
L-histidine tartrate	0.79	[18]

comparison is made between previously reported SHG results with LTT efficiency in Table 4.

3.10. Z-scan studies

The grown crystal of LTT is subjected to Z-scan analysis for determining the third order nonlinear parameters like nonlinear refractive index (n_2), nonlinear absorption coefficient (β) and nonlinear susceptibility ($\chi^{(3)}$). In Z-scan technique semiconductor laser (100 mW) was used as a source with wavelength 532 nm (green laser beam). The duration of laser pulse 10 ns with a beam diameter of 2.8 mm is used. The input laser beam was converted to polarize Gaussian beam by using a Gaussian filter and focused on the sample with thickness (L) 1 mm using a convex lens of focal length 103 mm. The sample is mounted on sample holder which tends to move along positive and negative directions in the Z-axis with beam propagation direction. After passing through sample the beam reaches the photodetector with a corresponding transmitted intensity which was recorded as a graph in the computer. The process can be carried in two methods closed aperture (CA) and open aperture (OA). In CA an aperture of some determined radius is placed in front of the detector, so the intensity of the beam purely depends on the radius of the aperture. In OA the beam directly passes through the lens, sample and reaches the detector where the intensity will be maximum to find out nonlinear absorption coefficient (β). The CA and OA curves of Z-scan are depicted in Figs. 12 and 13. The n_2 and β are directly proportional to the intensity of the incident beam. In CA the change in transmittance between peak and valley is measured as a self-focusing behavior [50]. In OA, β can be calculated [51].

To calculate the nonlinear refractive index (n_2) the Eq. (14) was used and it was calculated as 0.8466×10^{-12} (cm^2W^{-1}).

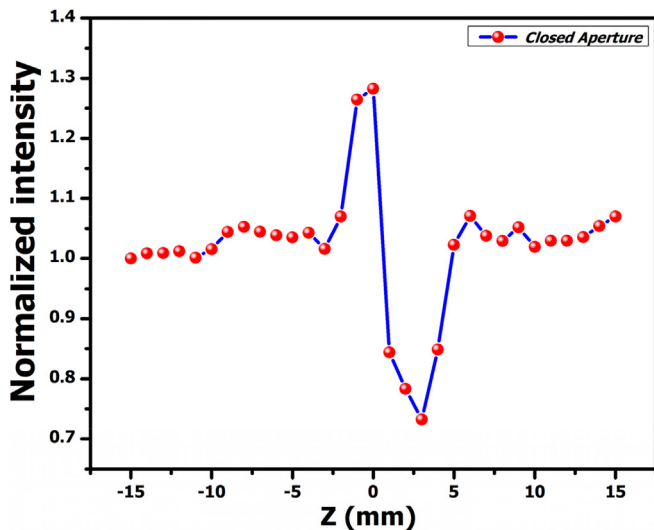


Fig. 12. Closed aperture (CA) spectrum of LTT crystal.

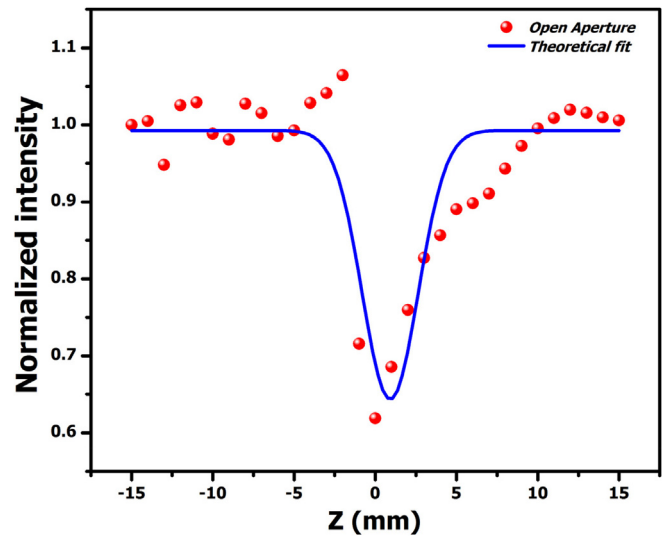


Fig. 13. Open aperture (OA) spectrum of LTT crystal.

$$n_2 = \frac{\Delta\phi}{kI_0L_{\text{eff}}} (m^2/W) \quad (14)$$

where ' $\Delta\phi$ ' is the axis phase shift, ' k ' is the wave number, ' I_0 ' is the intensity of the monochromatic source at the focus and ' L_{eff} ' is the effective thickness of the sample. To find the axis phase shift $\Delta\phi$ Eq. (18) was used and it was calculated as 2.04358 (radians).

$$|\Delta\phi| = \frac{\Delta T_{p-v}}{0.406(1-S)^{0.25}} \quad (18)$$

where ΔT_{p-v} is the difference between the normalized transmittance peak and valley transmittance of the CA curve. To find linear transmittance aperture (S), the Eq. (19) [52] was used and it was found to be 0.8069.

$$S = 1 - \exp\left(-\frac{2r_a^2}{w_a^2}\right) \quad (19)$$

where ' r_a ' is the radius of the aperture and ' w_a ' is the beam radius at aperture. To calculate the wave number k , expression (20) is used and it was found to be 11.8045×10^6 (radians per meter)

$$k = \frac{2\pi}{\lambda} (\text{rad/m}) \quad (20)$$

where ' λ ' is the wavelength of the monochromatic source. The effective thickness (L_{eff}) of the sample is calculated using Eq. (21) and it was found to be 0.9977 (mm).

$$L_{\text{eff}} = \frac{1 - e^{-\alpha L}}{\alpha} (\text{mm}) \quad (21)$$

where ' L ' is the thickness (1 mm) of the sample and ' α ' is the linear absorption coefficient. To calculate the nonlinear absorption coefficient (β) Eq. (22) is used and it was found to be 3.734×10^{-6} (mW^{-1}).

$$\beta = \frac{2\sqrt{2}\Delta T}{I_0L_{\text{eff}}} (m/W) \quad (22)$$

The value of β depends upon OA value, for two-photon absorption, the value will be in positive, for saturable absorption it will be negative [53]. In order to calculate the $\chi^{(3)}$ for real part ($\text{Re}\chi^{(3)}$) and imaginary part ($\text{Im}\chi^{(3)}$) [51] Eqs. (23) and (24) are used and the results found to be 0.38145×10^{-10} (electrostatic unit (or) Stat Coulomb) and 7.1266×10^{-10} (esu or StatC)

Table 5

Calculated Z- scan parameters of LTT crystal.

Parameters	Values
Nonlinear refractive index (n_2)	$0.84655 \times 10^{-12} \text{ cm}^2\text{W}^{-1}$
Nonlinear absorption co-efficient (β)	$3.734 \times 10^{-6} \text{ cmW}^{-1}$
Real part of the third-order susceptibility ($R_e(\chi^{(3)})$)	$0.3815 \times 10^{-10} \text{ esu}$
Imaginary part of the third-order susceptibility ($I_m(\chi^{(3)})$)	$7.1266 \times 10^{-10} \text{ esu}$
Third-order nonlinear optical susceptibility ($\chi^{(3)}$)	$7.1368 \times 10^{-10} \text{ esu}$

$$R_e\chi_{(esu)}^{(3)} = \frac{10^{-4}\epsilon_0 C^2 n_0^2 n_2}{\pi} (\text{cm}^2/\text{W}) \quad (23)$$

$$I_e\chi_{(esu)}^{(3)} = \frac{10^{-2}\epsilon_0 C^2 n_0^2 \lambda \beta}{\pi} (\text{cm}/\text{W}) \quad (24)$$

where ' ϵ_0 ' is the permittivity of free space $8.854 \times 10^{-12} \text{ C}^2\text{N}^{-1}\text{m}^{-2}$, ' C ' is the velocity of light in vacuum, ' n_0 ' is the refractive index of the LTT crystal. Using the following expression (25), the third order nonlinear susceptibility $\chi^{(3)}$ for the titular crystal is calculated and it is found to be 7.1368×10^{-10} (esu).

$$\chi^{(3)} = \sqrt{(R_e\chi^{(3)})^2 + (I_m\chi^{(3)})^2} \quad (25)$$

The LTT crystal provides a higher third-order nonlinear susceptibility ($\chi^{(3)}$) which attributed to the electron density transfer (donor to acceptor) within the molecular system [54]. The self-focalizing nature of the material is indicated by the positive sign of (n_2) [55], which lead the material as a promising agent for optical limiting and optical device fabrication [56–58]. The calculated parameters of Z- scan and their results are tabulated in Table 5.

4. Conclusion

Single crystal of L-threoninium tartrate with good optical transparency was grown by slow evaporation method. The orthorhombic system of the grown LTT crystal was confirmed using single crystal X-ray diffraction analysis. The functional group identification was carried out using FT-IR spectral analysis. The lower cut off wavelength of 190 nm is observed from UV-visible spectrum. The optical band gap was found to be 6.4 eV. Using transmittance data, optical parameters such as extension coefficient, reflectance and refractive index were obtained. The dielectric constant and loss were measured for various frequencies and temperatures. The mechanical parameters such as Vickers microhardness (H_v), Mayer index (n), yield strength (σ_y), elastic constant (C_{11}), fracture toughness (K_C) and Brittle index number (B_i) were calculated and found that the grown crystal belongs to hard category. The thermal study shows the grown crystal is thermally stable up to 257 °C, which is suitable for high energy lasing applications. The exact decomposition point was confirmed using auto melting point apertures and found to be 268 °C. The layer growth with 2D nucleation mechanism with less dislocation is confirmed by chemical etching analysis. The laser withstand capacity of the grown crystal was tested using laser damaged threshold analysis and the threshold value was found to be $6.57 \text{ GW}/\text{cm}^2$ which is a suitable for optical switching device fabrication. The NLO test reveals that the SHG efficiency is 2.91 times greater than the KDP crystal. Z-scan result reveals that the grown crystal possess relatively higher value of nonlinear refractive index (n_2) and nonlinear absorption coefficient (β) leads to larger value of third-order nonlinear optical susceptibility ($\chi^{(3)}$) which is apt for optical limiting applications. Therefore, the grown L-threoninium tartrate (LTT) crystal is novel material for optical limiting, optical switching and photonic device fabrications.

Acknowledgments

The authors are grateful to Dr. J. Danie Kingsley, Assistant Professor Senior, Department of Integrative Biology, SBST, VIT University, Vellore for providing etching studies. Dr. Vijayaragavan, Division of Physics, BS Abdur Rahman University, Chennai for providing NLO and LDT analysis. Archbishop Casimir Instrumentation center (ACIC), St Joseph's College, Tiruchirappalli for providing UV, FT-IR, thermal and di-electrical analysis. SAIF, IIT-Madras, Chennai for single crystal XRD analysis. Mr. K. Janardhanan and Mr. G. Stanly grateful for their technical and moral support. Dr. J.Samuel, Ms. Annie, Ms. Ivy and Ms. Ezhil for their constant support and encouragement.

Appendix A. Supplementary data

Supplementary data to this article can be found online at <https://doi.org/10.1016/j.mset.2019.05.003>.

References

- [1] S.M. Ravi Kumar, N. Melikechi, S. Selvakumar, P. Sagayaraj, Studies on the optical, thermal and electrical properties of Bis (thiourea) cadmium formate NLO crystals, *Physica B* 403 (2008) 4160–4163.
- [2] S.E. Allen Moses, S. Tamilselvan, S.M. Ravi Kumar, J. Johnson, Synthesis growth and characterization of semi-organic nonlinear optical L-threoninium sodium fluoride (LTSF) crystal for photonics application, *Chin. J. Phys.* 58 (2019) 294–302.
- [3] D. Vanitha, Sultan Asath Bahadur, Nallaperumal Nallamuthu, Athimoolam Shunmuganarayanan, A. Manikandan, Studies on conducting polymer blends: synthesis and characterizations of PVA/PVP doped with CaCl_2 , *J. Nanosci. Nanotechnol.* 18 (2018) 1723–1729.
- [4] D. Sivavishnu, R. Srineivasan, J. Johnson, Synthesis, growth, optical, band gap energy and mechanical properties of semiorganic nonlinear optical material: 2-aminopyridine potassium dihydrogen orthophosphate lithium chloride (2APKDP/L) crystal, *Mater. Sci. Energy Technol.* 1 (2018) 205–214.
- [5] Anusha Muthukumar, D. Arivuoli, E. Manikandan, M. Jayachandran, Enhanced violet photoemission of nanocrystalline fluorine doped zinc oxide (FZO) thin films, *Opt. Mater.* 47 (2015) 88–94.
- [6] K. Buse, A. Adibi, D. Psaltis, Non-volatile holographic storage in doubly doped lithium niobate crystals, *Int. J. Sci.* 393 (1998) 665–668.
- [7] E. Vinoth, S. Vetrivel, S. Gopinath, R. Aruljothi, T. Suresh, R.U. Mullai, A new class semi-organic nonlinear optical materials: mono(4-sulfo benzene aminium) tri nickel(II) bis(dihydrogen phosphate) for photonic applications, *Mater. Sci. Energy Technol.* 2 (2019) 234–245.
- [8] Petra Becker, Borate materials in nonlinear optics, *Adv. Mater.* 10 (1998) 979–992.
- [9] E. Manikandan, V. Murugan, G. Kavitha, P. Babu, M. Maaza, Nano flower rod wire-like structures of dual metal(Al and Cr) doped ZnO thin films: Structural, optical and electronic properties, *Mater. Lett.* 131 (2014) 225–228.
- [10] J. Johnson, R. Srineivasan, D. Sivavishnu, In depth study on growth aspects and characteristic properties of semiorganic nonlinear optical crystal: 4-Dimethylaminopyridine copper chloride, *Mater. Sci. Energy Technol.* 2 (2019) 226–233.
- [11] F.T. Thema, P. Beukes, B.D. Ngom, E. Manikandan, M. Maaza, Free standing diamond-like carbon thin films by PLD for laser based electrons/protons acceleration, *J. Alloys Compd.* 648 (2015) 326–331.
- [12] C. Razzetti, M. Ardoino, L. Zanotti, M. Zha, C. Paorici, Solution growth and characterisation of L-alanine single crystals, *Cryst. Res. Technol.* 37 (2002) 456–465.
- [13] A. Kandasamy, R. Mohan, M. Lydia Caroline, S. Vasudevan, Nucleation kinetics, growth, solubility and dielectric studies of L-proline cadmium chloride monohydrate semi organic nonlinear optical single crystal, *Cryst. Res. Technol.* 43 (2008) 186–192.
- [14] S.A. Martin Britto Dhas, S. Natarajan, Growth and characterization of L-prolinium tartrate – a new organic NLO material, *Cryst. Res. Technol.* 42 (2007) 471–476.
- [15] N. Renuka, N. Vijayan, Brijesh Rathi, R. Ramesh Babu, K. Nagarajan, D. Haranath, G. Bhagavannarayana, Synthesis growth and optical properties of semi organic nonlinear optical single crystal: L-Arginine acetate, *Optik* 123 (2012) 189–192.
- [16] G. Ramesh Kumar, S. Gokul Raj, R. Mohan, R. Jayavel, Growth and characterization of new nonlinear optical L-threoninium acetate single crystals, *J. Cryst. Growth* 283 (2005) 193–197.
- [17] S. Dhanuskodi, S. Manikandan, Spectral studies of methyl-p-hydroxy benzoate: an organic nonlinear optical crystalline material, *Cryst. Res. Technol.* 39 (2004) 586–591.
- [18] J.J. Rodrigues Jr., L. Misoguti, F.D. Nunes, C.R. Mendonca, S.C. Zilio, Optical properties of L-threonine crystals, *Opt. Mater.* 22 (2003) 235–240.

- [19] J. Mary Linet, S. Jerome Das, Optical mechanical and transport properties of unidirectional grown L-tartaric acid bulk single crystal for non-linear optical application, *Mater. Chem. Phys.* 126 (2011) 886–890.
- [20] S.A. Martin BrittoDhas, M. Suresh, G. Bhagavannarayana, S. Natarajan, Growth and characterization of L-Tartaric acid, an NLO material, *J. Cryst. Growth* 309 (2007) 48–52.
- [21] P. Christuraj, S. Anbarasu, P.S. Joseph, D. Prem Anand, Growth and characterization studies of L-threonine phosphate (LTP) a new semiorganic NLO crystal, *Optik* 126 (2015) 5517–5521.
- [22] Mohd. Shkir, V. Ganesh, S. AlFaify, H. Algarni, G. Bhagavannarayana, K.K. Maurya, M.M. Abutalib, I.S. Yahia, Bulk growth, structural, vibrational, crystalline perfection, optical and dielectric properties of L-threonine doped KDP single crystals grown by Sankaranarayanan-Ramasamy (SR) method, *Mater. Res. Innov.* (2016) 1–9.
- [23] B.S. Samuel, R. Krishnamurthy, R. Rajasekaran, Effect of L-aspartic acid on the growth, structure and spectral studies of zinc (tris) thiourea sulphate (ZTS) single crystals, *Spectrochim. Acta, Part A* 132 (2014) 526–532.
- [24] E. Manikandan, M.K. Moodley, S. Sinha Ray, B.K. Panigrahi, R. Krishnan, N. Padhy, K.G.M. Nair, A.K. Tyagi, Zinc oxide epitaxial thin film deposited over carbon on various substrate by pulsed laser deposition technique, *J. Nanosci. Nanotechnol.* 10 (2010) 5602–5611.
- [25] J. Tauc, *Amorphous and Liquid Semiconductors*, Plenum Press, London and New York, 1974.
- [26] D. Xue, K. Kitamura, Dielectric characterization of the defect concentration in lithium niobate single crystals, *Solid State Commun.* 122 (2002) 537–541.
- [27] A. Selvam, S. Pandi, V. Rajendran, S. Gnanam, S. Selvakumar, Growth and characterization of Urea succinic acid (USA) single crystal by using slow evaporation process, *Der PharmaChemica* 4 (2012) 228–233.
- [28] V. Parameswaran, N. Nallamuthu, P. Devendran, A. Manikandan, E.R. Nagarajan, Assimilation of NH₄Br in polyvinyl alcohol/poly(N-vinyl pyrrolidone) polymer blend-based electrolyte and its effect on ionic conductivity, *J. Nanosci. Nanotechnol.* 18 (2018) 944–3953.
- [29] B.R. Lawn, E.R. Fuller, Equilibrium penny-like cracks in indentation fracture, *J. Mater. Sci.* 10 (1975) 2016–2024.
- [30] J.H. Westbrook, Flow in rock salt structure Report 58-R L, 2033 of GE Research Laboratory, USA, 1958.
- [31] K. Sangwal, On the reverse indentation size effect and microhardness measurement of solid, *Mater. Chem. Phys.* 63 (2000) 145–152.
- [32] Tansuri Pal, Tanusree Kar, Studies on growth defects and mechanical properties of nonlinear optical crystal: L-arginine hydrofluoride, *J. Cryst. Growth* 276 (2005) 247–252.
- [33] E. Meyer, Contribution to the knowledge of hardness and hardness testing, *German Sci. J. Phys. (PhysikalischeZeitschrift)* 52 (1908) 740–835.
- [34] E.M. Onitsch, The present status of testing the hardness of materials, *Mikroskopie* 95 (1956) 12–14.
- [35] O. Sahin, O. Uzun, U. Kolemen, B. Duzgun, N. Ucar, Indentation size effect and microhardness study of β -Sn single crystals, *Chin. Phys. Lett.* 22 (2005) 3137–3140.
- [36] P. Manikandan, D. Manikandan, E. Manikandan, A. Christy Ferdinand, Structural optical and micro-Raman scattering studies of nanosized copper ion (Cu⁺) exchanged soda lime glasses, *Plasmonics* 9 (2014) 637–643.
- [37] R. Surekha, R. Gunaseelan, P. Sagayaraj, K. Ambujam, L-Phenylalanine L-phenylalanine bromide – a new nonlinear optical material, *CrystEngComm* 34 (2014) 7979–7989.
- [38] M. Mahadevan, P. Anandan, K. Ramachandran, M. Arivandhan, Y. Hayakawa, Studies on the growth aspects and characterization of sodium para-nitro phenolate single crystals for nonlinear optical applications, *Optik* 125 (2014) 5515–5518.
- [39] V. Parameswaran, N. Nallamuthu, P. Devendran, E.R. Nagarajan, A. Manikandan, Electrical conductivity studies on Ammonium bromide incorporated with Zwitterionic polymer blend electrolyte for battery application, *Physica B* 515 (2017) 89–98.
- [40] M. Rajalakshmi, R. Indirajith, M. Palanichamy, R. Gopalakrishnan, Synthesis, growth, thermal, optical and mechanical properties of 2-Aminopyridinium 4-methylbenzoate Dihydrate, *Spectrochim. Acta, Part A* 84 (2011) 43–50.
- [41] G.C. Bhar, A.K. Chaudhury, P. Kumbhakar, Study of laser induced damage threshold and effect of inclusions in some nonlinear crystals, *Appl. Surf. Sci.* 161 (2000) 155–162.
- [42] N.L. Boling, M.D. Crisp, G. Dube, Laser-induced surface damage, *Appl. Opt.* 12 (1973) 650–660.
- [43] S.K. Sharma, Sunil Verma, K.S. Yeshpal Singh, M.K. Bartwal, G.S. Tiwari, Lodha and G. Bhagavannarayana, Investigations of structural defects, crystalline perfection, metallic impurity concentration and optical quality of flat-top KDP crystal, *Opt. Mater.* 46 (2015) 329–338.
- [44] N. Vijayan, G. Bhagavannarayana, T. Kanagasakaran, R. Ramesh Babu, R. Gopalakrishnan, P. Ramasamy, Crystallization of benzimidazole by solution growth method and its characterization, *Cryst. Res. Technol.* 41 (2006) 784–789.
- [45] Redrothu Hanumantharao, S. Kalainathan, Impact of pH of L-threonine single crystals on optical parameters and laser damage threshold energy, *Int. J. Chemtech Res.* 4 (2012) 1478–1484.
- [46] S.E. Allen Moses, S. Tamilselvan, S.M. Ravikumar, G. Vinita, Tejaswi Ashok Hegde, G.J. Shanmuga Sundar, M. Vimalan, S. Sivaraj, Crystal structure, spectroscopic, thermal, mechanical, linear optical, second order and third order nonlinear optical properties of semiorganic crystal: L-threonine phosphate (LTP), *J. Mater. Sci.* (2019), <https://doi.org/10.1007/s10854-019-01229-9>.
- [47] S.K. Kurtz, T.T. Perry, A powder technique for the evaluation of nonlinear optical material, *J. Appl. Phys.* 39 (1968) 3798–3813.
- [48] S.A. Martin Britto Dhas, G. Bhagavannarayana, S. Natarajan, Growth and characterization of a new potential NLO material from the amino acid family-L-proline picrate, *J. Cryst. Growth* 310 (2008) 3535–3539.
- [49] T. Uma Devi, N. Lawrence, R. Ramesh Babu, K. Ramamurthi, Growth and characterization of L-proline picrate single crystal: a promising NLO crystal, *J. Cryst. Growth* 310 (2008) 116–123.
- [50] Indrajit Bhattacharyya, Shekhar Priyadarshi, Debabrata Goswami, Molecular structure-property correlations from optical nonlinearity and thermal-relaxation dynamics, *Chem. Phys. Lett.* 469 (2009) 104–109.
- [51] Eric W. Van Stryland, Mansoor Sheik-Bahae, Z-scan measurements of optical nonlinearities, *Character. Tech. Tabulations Org. Nonlinear Mater.* 60 (1998) 655–692.
- [52] Seetharam Shettigar, G. Umesh, K. Chandrasekharan, Balakrishna Kalluraya, Third order nonlinear optical properties and two photon absorption in newly synthesized phenyl sydnone doped polymer, *Synth. Metals* 157 (2007) 142–146.
- [53] Mansoor Sheik-Bahae, Ali A. Said, T.-H. Wei, David J. Hagan, Eric W. Van Stryland, Sensitive measurement of optical nonlinearities using a single beam, *IEEE J. Quantum Electr.* 26 (1990) 760–769.
- [54] K. Naseema, M. Shyma, K.B. Manjunatha, A. Muralidharan, G. Umesh, Vijayalakshmi Rao, $\chi^{(3)}$ measurement and optical limiting studies of urea picrate, *Opt. Laser Technol.* 43 (2011) 1286–1291.
- [55] D. Wolfersberger, N. Fressengeas, J. Maufroy, G. Kugel, Laser beam self-focusing in photorefractive materials: optical limiting application, *J. Nonlinear Opt. Phys. Mater.* 9 (2000) 441–450.
- [56] Z. Zang, All-optical switching in Sagnac loop mirror containing an ytterbium-doped fiber and fiber Bragg grating, *Appl. Opt.* 52 (2013) 5701–5706.
- [57] Z. Zang, Y. Zhang, Analysis of optical switching in a $\chi^{(2)}$ doped fiber Bragg grating by using self-phase modulation and cross-phase modulation, *Appl. Opt.* 51 (2012) 3424–3430.
- [58] Zhi-Gang Zang, Yu-Jun Zhang, Low-switching power optical bistability based on optical nonlinearity of ytterbium-doped fiber with a fiber Bragg grating pair, *J. Mod. Opt.* 59 (2012) 161–165.